

Fermi gas behavior of a one-dimensional metallic band of Pt-induced nanowires on Ge(001)

K. Yaji,^{1,*} I. Mochizuki,² S. Kim,¹ Y. Takeichi,² A. Harasawa,¹ Y. Ohtsubo,³ P. Le Fèvre,³ F. Bertran,³ A. Taleb-Ibrahimi,^{3,4} A. Kakizaki,¹ and F. Komori¹

¹*Institute for Solid State Physics, The University of Tokyo, 5-1-5 Kashiwanoha, Kashiwa, Chiba 277-8581, Japan*

²*Institute of Materials Structure Science, High Energy Accelerator Research Organization (KEK), 1-1 Oho, Tsukuba, Ibaraki 305-0801, Japan*

³*Synchrotron SOLEIL, L'Orme des Merisiers, Saint-Aubin-BP 48, F-91192 Gif sur Yvette, France*

⁴*URI/CNRS Synchrotron SOLEIL, Saint-Aubin, F-91192 Gif sur Yvette, France*

(Received 15 April 2013; revised manuscript received 22 May 2013; published 27 June 2013)

We have investigated the electronic band structure of Pt-induced nanowires on Ge(001) [Pt/Ge(001) NWs] by angle-resolved photoelectron spectroscopy at 6 K. Single-domain samples of Pt/Ge(001) NWs were prepared on vicinal Ge(001) substrates. One of the bands disperses only in the nanowire direction, and its Fermi surface consists of strictly straight lines, indicating that it is an ideal one-dimensional metallic state. An energy distribution curve of the one-dimensional band is explained by a Fermi-Dirac-type spectral shape, which is against both a Luttinger liquid and Peierls instability schemes.

DOI: [10.1103/PhysRevB.87.241413](https://doi.org/10.1103/PhysRevB.87.241413)

PACS number(s): 73.20.Mf, 68.47.Fg, 71.10.Pm, 79.60.-i

Electrons in one-dimensional metals exhibit intriguing physics such as a Luttinger liquid^{1,2} and Peierls instability.^{3,4} According to the framework of Luttinger liquid, the strong Coulomb interaction of one-dimensional electrons makes a Fermi-liquid state unstable.² Experimental observations of the Luttinger liquid in carbon nanotube⁵ and organic conductor TTF-TCNQ⁶ by angle-resolved photoelectron spectroscopy (ARPES) are typical examples, where the photoelectron intensities $I(E)$ follow a power-law dependence on the binding energy near the Fermi energy (E_F), [$I(E) \propto |E - E_F|^\alpha$]. On the other hand, in the scenario of Peierls instability, the lattice is periodically distorted and an energy gap opens at E_F because of electron-phonon coupling.

One-dimensional nanowires formed by metal atoms adsorbed on semiconductor surfaces have been offering an opportunity to investigate such phenomena of one-dimensional electrons. For instance, silicon (Si) and germanium (Ge) surfaces covered with submonolayer metal atoms, such as indium (In) and gold (Au), have been extensively studied by ARPES.⁷⁻¹⁵ The Fermi surfaces of In/Si(111) and Au/Si(553) show two-dimensional undulation due to some inter-chain interactions.^{7,8,11} The electronic states are not ideal one-dimensional states but quasi-one-dimensional states. The former undergoes a metal-insulator transition at a structural phase transition temperature, and a Peierls transition has been discussed. In the case of Au/Si(557), the Fermi surface consists of split-straight lines.¹² The splitting was first attributed to spinon-holon bands which are characteristic of a Luttinger liquid.⁹ However, this interpretation was ruled out later by the observation of two separate Fermi-level crossings, indicating a Fermi gas state.¹⁰ For Au/Ge(001), on the other hand, a power-law spectral shape observed near the Fermi level was recently attributed to a Luttinger liquid.^{14,15}

Electrons in the nanowires are strongly influenced by defects, irregularly lying on the surface and cutting the nanowires into short segments. Line shapes of photoelectron spectra of one-dimensional metallic nanowires also depend on

the defects density.^{16,17} For example, the Au/Si(557) surface shows high density of defects, giving a mean length of the interrupted chains of 5 nm.¹² Longer segments are required for clarifying if the nanowires at surfaces exhibit the Luttinger liquid behavior, or Peierls instability.

Platinum (Pt)-induced nanowires formed on Ge(001) substrates [Pt/Ge(001) NWs] are suitable for investigation of the one-dimensional electrons because Pt/Ge(001) nanowires (NWs) exhibit defect- and kink-free surface reconstruction, where the mean length on the nanowires is of the order of several hundreds of nm.¹⁸⁻²¹ Figures 1(a) and 1(b) show a structure model of Pt/Ge(001) NWs proposed by reflection high-energy positron diffraction (RHEPD) analysis.²¹ In this model, there are Ge dimers in the topmost layer, and Pt atoms are embedded in the second and fourth layers. In addition, Pt/Ge(001) NWs show a structural phase transition between a high-temperature (HT) phase with a $p(4 \times 2)$ periodicity and a low-temperature (LT) phase with a $p(4 \times 4)$ periodicity at 80 K, where an alternate buckling of two Ge dimers in the two adjacent $p(4 \times 2)$ unit cells has been found.²¹ Concerning the electronic properties, the investigation with scanning tunneling spectroscopy proposed metallic states of Pt/Ge(001) NWs.^{18,22,23} However, the electronic band structure and the Fermi surface have not been clarified up to now.

In this Rapid Communication, we report the ground-state electronic properties of Pt/Ge(001) NWs studied by ARPES at 6 K, a sufficiently lower temperature than the phase transition. Single-domain samples of Pt/Ge(001) NWs on vicinal Ge(001) substrates were used to make clear the shape of the band structure in a surface Brillouin zone (SBZ). The surface structure was confirmed by low-energy electron diffraction (LEED) and scanning tunneling microscopy (STM). Two metallic bands associated with Pt/Ge(001) NWs were observed and one of them exhibits an ideal one-dimensional behavior. We reveal that the electrons in the one-dimensional band exhibit Fermi gas behavior.

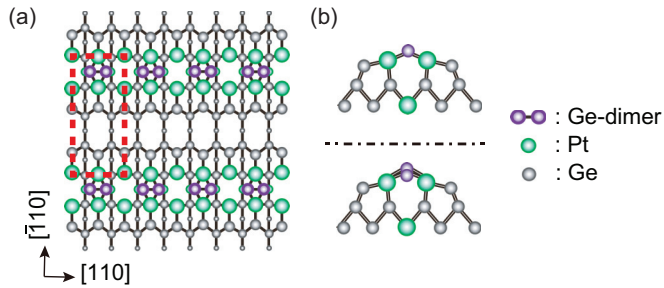


FIG. 1. (Color online) (a) Top view of the surface structure model of Pt/Ge(001) NWs proposed by RHEPD.²¹ Dashed rectangle represents a $p(4 \times 2)$ unit cell of the HT phase. (b) Side views of the structure model of Pt/Ge(001) NWs, where the structural models of the HT and LT phases are shown in the upper and lower panels, respectively.

Experiments using LEED, STM, and ARPES were performed in ultrahigh-vacuum systems. We used *n*-type vicinal Ge(001) wafers, where the substrates were tilted toward the $[\bar{1}10]$ direction by 2° . The clean Ge(001) surface was obtained by several cycles of 0.8 keV Ar^+ bombardment at 670 K and subsequent annealing up to 900 K for a few minutes. Platinum was deposited onto the clean substrate from an electron-bombardment-type evaporator. The substrate temperature during the deposition was optimized between 620 and 720 K, depending on the Pt coverage, in order to make a well-ordered single-domain Pt/Ge(001) NWs surface in a wide area. The amount of deposited Pt was adjusted by checking the sharpness of the LEED spots. Images of the surfaces were acquired by an STM (Omicron VTSTM) at room temperature (RT) in a constant-current mode. A hemispherical electron energy analyzer (VG Scienta R4000) was used for the ARPES measurements at Cassiopée beamline at synchrotron SOLEIL. All spectra were measured at photon energy $h\nu = 25$ eV with linearly polarized light, of which the electric-field vector was perpendicular to the light-incident plane which coincides with a (110) plane of the substrate. The total-energy resolution was set to 30 meV. The sample temperature was kept at 6 K during the ARPES measurements.

Figure 2(a) exhibits a typical LEED pattern from Pt/Ge(001) NWs on the vicinal substrate at RT. A LEED pattern from Pt/Ge(001) NWs on a flat Ge(001) substrate is also shown for comparison in Fig. 2(b). The latter indicates the presence of a double-domain $p(4 \times 2)$ surface. In contrast, on the vicinal substrate, the $p(4 \times 2)$ periodicity is prominent only in one direction, and the $2 \times$ periodicity of the major domains is perpendicular to the miscut direction.

Figures 2(c) and 2(d) show the STM images of Pt/Ge(001) NWs formed on the vicinal Ge(001) substrate with image sizes of 400×400 nm² and 130×130 nm², respectively. Step edges are parallel to the $[110]$ direction. The bright protrusions in the images are identified as Ge dimers lying in the topmost layer. It is found that single-domain nanowire arrays with single domain cover more than 90% of the surface. We confirmed that there are very few point defects on the nanowires as in the previously reported STM images.^{20,21} The majority of the area is covered with the nanowires parallel to the step edges. In Fig. 2(c), the areas surrounded by bold lines are minority

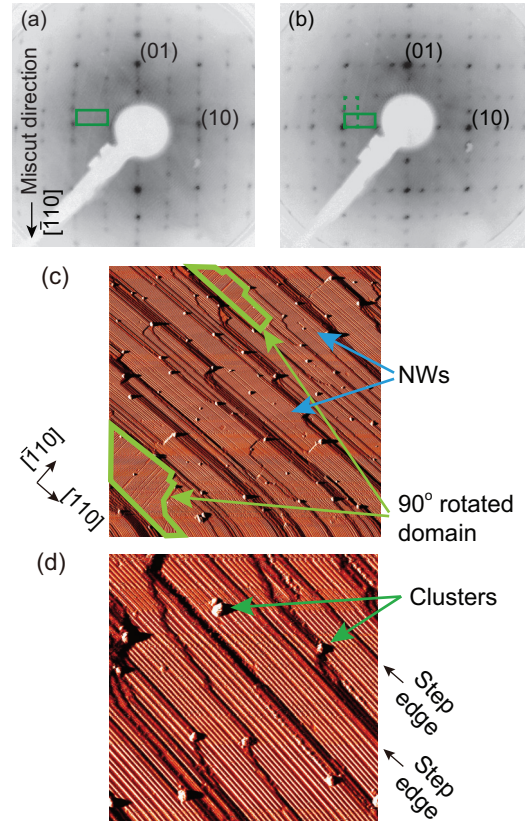


FIG. 2. (Color online) (a), (b) LEED patterns of Pt/Ge(001) NWs on vicinal (a) and flat (b) Ge(001) substrates at RT. The primary electron energy was set to 128 eV. An arrow in (a) represents the miscut direction of the vicinal surface. The unit cell of each domain is presented with solid and dashed rectangles in the images. (c) Large-scale STM image (400×400 nm²) of Pt/Ge(001) NWs on the vicinal Ge(001) substrate. Most of wide terraces are covered by the nanowires parallel to the step edges. The areas surrounded by bold lines (green) represent minority domains. (d) Magnified STM image (130×130 nm²). The protrusions (white) correspond to the Ge dimers in the topmost layer. In both images, the bias voltage is 1.5 V and the tunneling current 0.5 nA.

domains, where the nanowires are aligned perpendicularly to the step edges. These perpendicular domains cover less than 10% of the surface. In addition, we can recognize that the region of α and β terraces^{18,19} covers less than a few percent of the surface. The spectra from these terraces can then be neglected in the ARPES measurements. We thus confirm that the well-ordered single-domain samples of Pt/Ge(001) NWs are grown on a vicinal surface.

We have recorded an ARPES intensity map in order to clarify the dimensionality of the surface-state bands of Pt/Ge(001) NWs. Figure 3(a) shows the Fermi-surface mapping in the second and third SBZs on the single-domain surface at 6 K. The image was obtained by the summation of the photoelectron intensity within a 10-meV energy window centered at E_F . The boundaries of the SBZs of the $p(4 \times 2)$ periodicity at the HT phase and of the $p(4 \times 4)$ periodicity at the LT phase are represented by thin dashed and solid lines, respectively. Photoelectron intensity is enhanced in the third SBZ while

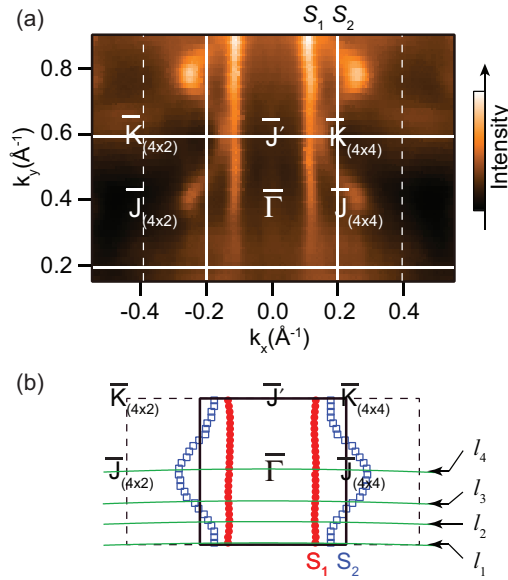


FIG. 3. (Color online) (a) Constant energy ARPES map at E_F of Pt/Ge(001) NWs with the single-domain surface formed on the vicinal Ge(001) substrate. The photoelectron intensity is represented by color scale. Thin solid and dashed lines denote the boundaries of the SBZs of $p(4 \times 4)$ and $p(4 \times 2)$, respectively. (b) Peak position plots from the MDCs at E_F in the third SBZ. Circles and squares correspond to the S_1 and S_2 bands, respectively. Lines l_1 – l_4 represent the wave vector cuts of ARPES images shown in Figs. 4(a)–4(d), respectively.

it is rather weak in the first SBZ. Peak positions extracted from the momentum distribution curves (MDCs) at E_F are also shown in Fig. 3(b). Note that the k_x (k_y) corresponds to the parallel (perpendicular) direction to the NWs.

From the Fermi-surface image, we can clearly identify two metallic surface bands labeled S_1 and S_2 . The Fermi surface of S_1 consists of straight lines in the k_y direction. This means that the S_1 band disperses predominantly in the nanowire direction, and that there is a very weak dispersion in the direction perpendicular to the nanowires. The measured Fermi wave vector of S_1 is 0.118 \AA^{-1} on the $\bar{\Gamma}\bar{J}_{(4 \times 4)}$ ($\bar{\Gamma}\bar{J}_{(4 \times 2)}$) and $\bar{J}'\bar{K}_{(4 \times 4)}$ ($\bar{J}'\bar{K}_{(4 \times 2)}$) axes, and 0.114 \AA^{-1} in the middle between the $\bar{\Gamma}\bar{J}_{(4 \times 4)}$ and $\bar{J}'\bar{K}_{(4 \times 4)}$ axes. The amplitude of the two-dimensional undulation of S_1 around the straight line, which indicates a deviation from a purely one-dimensional Fermi surface, is less than 1% with respect to the size of the SBZ. The two-dimensional undulation of S_1 at E_F is thus negligibly small, and the S_1 band is an ideal one-dimensional metallic state which is electronically decoupled from neighboring wires. We note that the one-dimensional feature of S_1 is kept at least down to 0.2 eV below E_F in the observed ARPES intensity map. The two-dimensional undulation of the S_1 band, however, becomes larger at binding energies higher than 0.2 eV. The Fermi surface of S_2 shows a two-dimensional undulation. The measured Fermi wave vector of S_2 is 0.255 \AA^{-1} on the $\bar{\Gamma}\bar{J}_{(4 \times 4)}$ ($\bar{\Gamma}\bar{J}_{(4 \times 2)}$) axis, and is 0.157 \AA^{-1} on the $\bar{J}'\bar{K}_{(4 \times 4)}$ ($\bar{J}'\bar{K}_{(4 \times 2)}$) axis.

Figures 4(a)–4(d) show the band structures of Pt/Ge(001) NWs recorded along lines l_1 – l_4 shown in Fig. 3(b). A schematic drawing of the S_1 and S_2 bands in the (k_x, k_y)

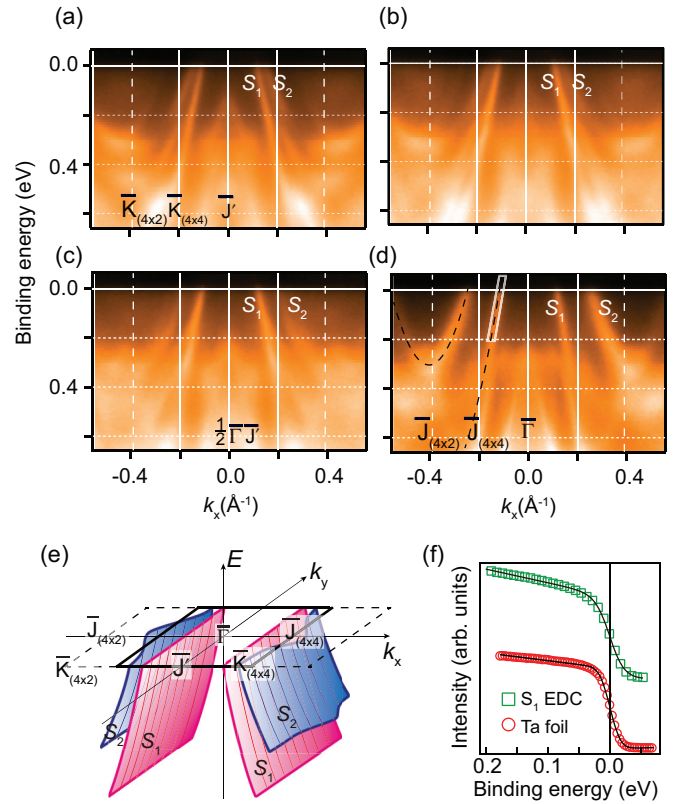


FIG. 4. (Color online) (a)–(d) ARPES images taken along thin solid (green) lines, l_1 – l_4 , shown in Fig. 3(b), where l_1 , l_2 , l_3 , and l_4 correspond to $k_y = 0.60, 0.64, 0.69, 0.78 \text{ \AA}^{-1}$ on the $\bar{\Gamma}\bar{J}'$ axis, respectively. Dashed curves in (d) represent the band structures of S_1 and S_2 , which were fitted to the data.²⁴ (e) Schematic drawing of the S_1 and S_2 bands. (f) (Top) The integrated EDC of S_1 near E_F . A thin solid parallelogram shown in (d) represents an extracted E - k_x plane to obtain an EDC for a k_y slice. The EDC with the E - k_x plane is integrated over k_y in the SBZ. (Bottom) The Fermi edge (red circles) taken from Ta foil. Solid curves represent fitting results with the Fermi distribution function and polynomial background.

space is shown in Fig. 4(e). The S_1 band exhibits a steep dispersion and crosses the Fermi level in the projected bulk band gap. The effective mass of S_1 is estimated to be $0.35m_e$ at E_F .²⁴ The shape of S_1 in each slice in the E - k_x plane is completely identical within 0.2 eV below E_F . This means that the S_1 band is strictly one-dimensional between E_F and 0.2 eV below E_F , and isolated in the bulk band gap. On the other hand, S_1 is not clearly observed at binding energies higher than 0.3 eV because of the existence of some bulk-derived states and increased background intensity. The dispersion of S_2 suggests a free-electron-like parabolic band, of which the backfolding points are found on the $\bar{J}_{(4 \times 2)}\bar{K}_{(4 \times 2)}$ axis. The effective mass of S_2 is estimated to be $0.32m_e$ on the $\bar{\Gamma}\bar{J}$ axis.²⁴

The surface periodicity of Pt/Ge(001) NWs in the LT phase is $p(4 \times 4)$, which is explained by an alternative buckling of the topmost Ge dimers.²¹ However, the backfolding for S_1 and S_2 reflecting the $p(4 \times 4)$ periodicity is invisible in the ARPES images and the Fermi surfaces. Thus, the contribution of the topmost Ge dimers to the S_1 and S_2 states is negligibly small. The orbital characters of S_1 and S_2 might be attributed mainly

to the Pt atoms embedded in the fourth layer of the model shown in Fig. 1 rather than to the Ge dimers.

Metallicity of one-dimensional metallic bands in one-dimensional nanowires on the semiconductor surfaces is often lost upon cooling. This is explained by the Peierls instability scheme, in which a metal-insulator transition is driven by electron-phonon coupling, as reported on In/Si(111) and Au/Si(557).^{25,26} The surface structural phase transition of Pt/Ge(001) NWs was also interpreted as the Peierls transition on the basis of STM studies.²⁷ However, we have found no gap opening of S_1 and S_2 at the Fermi energy in the LT phase. We notice that the Fermi wave vectors of S_1 and S_2 deviate largely from a nesting vector of $Q = 0.39 \text{ \AA}^{-1}$. Therefore, S_1 and S_2 do not directly contribute to the structural phase transition and are stable against the Peierls instability if it exists. The electron-phonon interaction could not be strong enough to induce any structural transition with the nesting vector for S_1 by the Peierls instability scheme.

Next, we examine whether or not the one-dimensional metallic band S_1 exhibits a Luttinger liquid behavior. Figure 4(f) shows an integrated energy distribution curve (EDC) of S_1 near the Fermi energy, where the ARPES intensity for S_1 is integrated over k_y in the SBZ. A spectrum taken from a Ta foil (a three-dimensional conventional metal), measured with an energy resolution of 30 meV at 6 K, is also shown with circles for comparison. The intensity of S_1 at E_F is to be exactly half value of the actual peak height due to the Fermi distribution function, which is similar to the intensity from the Ta foil. In addition, there is no unusual suppression of the intensity in the energy range just below E_F . The result is quite different from the Luttinger-type power-law shape. We therefore conclude that the EDC of S_1 is well explained by a Fermi-Dirac-type spectral shape and the electron in S_1 behaves as expected in a one-dimensional Fermi gas.

We observed non-Luttinger-liquid behavior for S_1 , despite the fact that S_1 shows an ideal one-dimensional metallic band. This result is quite different from the findings for

the Au/Ge(001) systems.^{14,15} For a Luttinger liquid scheme, one assumes that one-dimensional electrons are completely isolated from other carriers. In other words, the collective excitation of one-dimensional electrons results from the absence of screening effect and any other interaction by the other carriers. For Pt/Ge(001) NWs, the free-electron-like S_2 band is found. The electrons in S_2 can thus provide an effective screening for the collective excitation of the electrons in S_1 . On the other hand, in the case of Au/Ge(001), electrons can undergo a Luttinger liquid behavior without any screening effect because the surface exhibits a single metallic band.¹³

In summary, we have studied the electronic property of defect- and kink-free Pt/Ge(001) NWs by ARPES. We have prepared single-domain samples on the vicinal Ge(001) substrates. The surface structure was confirmed by LEED and STM, where the nanowires are aligned parallel to the step edges on the vicinal substrate. Two metallic bands associated with Pt/Ge(001) NWs were observed at 6 K. The S_1 band exhibits strictly straight Fermi lines and steeply disperses only in the nanowire direction. This is direct evidence that S_1 is an ideal one-dimensional metallic state. However, the EDC of S_1 at E_F is not suppressed and the spectral shape is consistent with a Fermi-Dirac-type distribution function. We therefore conclude that the electron in the S_1 band behaves not as a Luttinger liquid but as a one-dimensional Fermi gas. The S_2 band, on the other hand, has an open Fermi surface consisting of wavy lines.

The authors acknowledge J. Pinon and D. Ragonnet for their technical support during the experiments at the Cassiopée beamline at synchrotron SOLEIL. The present work was partly supported by Bilateral Joint Research Project between Japan (JSPS) and France (CNRS). This work was also financially supported by the JSPS Grant-in-Aid for Young Scientists (B), Grant No. 24740197. It was partly performed at BL-19A, KEK Photon Factory, Japan (PF-PAC Grant No. 2011G085).

*yaji@issp.u-tokyo.ac.jp

¹J. M. Luttinger, *J. Math. Phys. (NY)* **4**, 1154 (1963).

²J. Voit, *Rep. Prog. Phys.* **58**, 977 (1995).

³R. E. Peierls, *Quantum Theory of Solids* (Clarendon, Oxford, 1955).

⁴P. C. Snijders and H. H. Weitering, *Rev. Mod. Phys.* **82**, 307 (2010).

⁵H. Ishii, H. Kataura, H. Shiozawa, H. Yoshioka, H. Otsubo, Y. Takayama, T. Miyahara, S. Suzuki, Y. Achiba, M. Nakatake, T. Narimura, M. Higashiguchi, K. Shimada, H. Namatame, and M. Taniguchi, *Nature (London)* **420**, 540 (2003).

⁶R. Claessen, M. Sing, U. Schwingenschlögl, P. Blaha, M. Dressel, and C. S. Jacobsen, *Phys. Rev. Lett.* **88**, 096402 (2002).

⁷H. W. Yeom, K. Horikoshi, H. M. Zhang, K. Ono, and R. I. G. Uhrberg, *Phys. Rev. B* **65**, 241307(R) (2002).

⁸J. R. Ahn, J. H. Byun, H. Koh, E. Rotenberg, S. D. Kevan, and H. W. Yeom, *Phys. Rev. Lett.* **93**, 106401 (2004).

⁹P. Segovia, D. Purdie, M. Hengsberger, and Y. Baer, *Nature (London)* **402**, 504 (1999).

¹⁰R. Losio, K. N. Altmann, A. Kirakosian, J.-L. Lin, D. Y. Petrovykh, and F. J. Himpsel, *Phys. Rev. Lett.* **86**, 4632 (2001).

¹¹J. N. Crain, A. Kirakosian, K. N. Altmann, C. Bromberger, S. C. Erwin, J. L. McChesney, J.-L. Lin, and F. J. Himpsel, *Phys. Rev. Lett.* **90**, 176805 (2003).

¹²J. N. Crain, J. L. McChesney, F. Zheng, M. C. Gallagher, P. C. Snijders, M. Bissen, C. Gundelach, S. C. Erwin, and F. J. Himpsel, *Phys. Rev. B* **69**, 125401 (2004).

¹³K. Nakatsuji, R. Niikura, Y. Shibata, M. Yamada, T. Iimori, and F. Komori, *Phys. Rev. B* **80**, 081406(R) (2009).

¹⁴C. Blumenstain, J. Schäfer, S. Mietke, S. Meyer, A. Dollinger, M. Lochner, X. Y. Cui, L. Patthey, R. Matzdorf, and R. Claessen, *Nat. Phys.* **7**, 776 (2011).

¹⁵S. Meyer, J. Schäfer, C. Blumenstein, P. Höpfner, A. Bostwick, J. L. McChesney, E. Rotenberg, and R. Claessen, *Phys. Rev. B* **83**, 121411(R) (2011).

¹⁶P. Starowicz, O. Gallus, Th. Pillo, and Y. Baer, *Phys. Rev. Lett.* **89**, 256402 (2002).

¹⁷A. S. Rodin and M. M. Fogler, *Phys. Rev. Lett.* **105**, 106801 (2010).

- ¹⁸O. Gürü, O. A. O. Adam, H. J. W. Zandvliet, and B. Poelsema, *Appl. Phys. Lett.* **83**, 4610 (2003).
- ¹⁹M. Fischer, A. van Houselt, D. Kockmann, B. Poelsema, and H. J. W. Zandvliet, *Phys. Rev. B* **76**, 245429 (2007).
- ²⁰J. Schäfer, S. Meyer, C. Blumenstein, K. Roensch, R. Claessen, S. Mietke, M. Klinke, T. Podlich, R. Matzdorf, A. A. Stekolnikov, S. Sauer, and F. Bechstedt, *New J. Phys.* **11**, 125011 (2009).
- ²¹I. Mochizuki, Y. Fukaya, A. Kawasuso, K. Yaji, A. Harasawa, I. Matsuda, K. Wada, and T. Hyodo, *Phys. Rev. B* **85**, 245438 (2012).
- ²²J. Schäfer, D. Schrupp, M. Preisinger, and R. Claessen, *Phys. Rev. B* **74**, 041404(R) (2006).
- ²³A. A. Stekolnikov, F. Bechstedt, M. Wisniewski, J. Schäfer, and R. Claessen, *Phys. Rev. Lett.* **100**, 196101 (2008).
- ²⁴See Supplemental Material at <http://link.aps.org/supplemental/10.1103/PhysRevB.87.241413> for estimation of the effective mass.
- ²⁵H. W. Yeom, S. Takeda, E. Rotenberg, I. Matsuda, K. Horikoshi, J. Schaefer, C. M. Lee, S. D. Kevan, T. Ohta, T. Nagao, and S. Hasegawa, *Phys. Rev. Lett.* **82**, 4898 (1999).
- ²⁶J. R. Ahn, H. W. Yeom, H. S. Yoon, and I.-W. Lyo, *Phys. Rev. Lett.* **91**, 196403 (2003).
- ²⁷A. van Houselt, T. Gnielka, J. M. J. Aan de Brugh, N. Oncel, D. Kockmann, R. Heid, K. P. Bohnen, B. Poelsema, and H. J. W. Zandvliet, *Surf. Sci.* **602**, 1731 (2008).